

Reaction Mechanism Governing Formation of 1,3-Bis(diphenylphosphino)propane-Protected Gold Nanoclusters

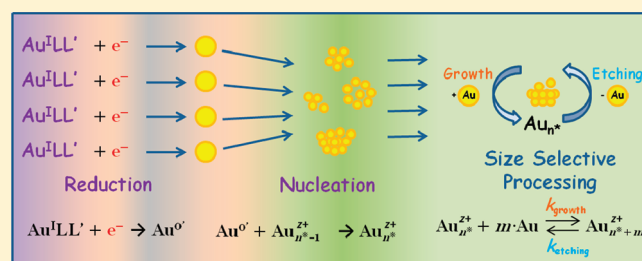
Jeffrey W. Hudgens,^{*,†} John M. Pettibone,[‡] Thomas P. Senftle,^{‡,§} and Ryan N. Bratton^{‡,||}

[†]Biochemical Science Division and [‡]Chemical and Biochemical Reference Data Division National Institute of Standards and Technology, Gaithersburg, Maryland 20899, United States

S Supporting Information

ABSTRACT: This report outlines the determination of a reaction mechanism that can be manipulated to develop directed syntheses of gold monolayer-protected clusters (MPCs) prepared by reduction of solutions containing 1,3-bis(diphenylphosphino)propane (L^3) ligand and $Au(PPh_3)Cl$. Nanocluster synthesis was initiated by reduction of two-coordinate phosphine-ligated $[Au^I LL']^+$ complexes ($L, L' = PPh_3, L^3$), resulting in free radical complexes. The $[Au^0 LL']^0$ free radicals nucleated, forming a broad size distribution of ligated clusters. Timed UV–vis spectroscopy and electrospray ionization mass spectrometry monitored the ligated Au_x , $6 \leq x \leq 13$, clusters, which comprise reaction intermediates and final products. By employing

different solvents and reducing agents, reaction conditions were varied to highlight the largest portion of the reaction mechanism. We identified several solution-phase reaction classes, including dissolution of the gold precursor, reduction, continuous nucleation/core growth, ligand exchange, ion–molecule reactions, and etching of colloids and larger clusters. Simple theories can account for the reaction intermediates and final products. The initial distribution of the nucleation products contains mainly neutral clusters. However, the rate of reduction controls the amount of reaction overlap occurring in the system, allowing a clear distinction between reduction/nucleation and subsequent solution-phase processing. During solution-phase processing, the complexes undergo core etching and core growth reactions, including reactions that convert neutral clusters to cations, in a cyclic process that promotes formation of stable clusters of specific metal nuclearity. These processes comprise “size-selective” processing that can narrow a broad distribution into specific nuclearities, enabling development of tunable syntheses.



INTRODUCTION

Gold monolayer-protected clusters (MPCs) contain extraordinary technological potential, and their unique physicochemical properties can be tuned as a function of gold nuclearity or ligand cap. Enormous effort has been invested developing methods for producing specific gold nuclearity clusters, but progress toward syntheses with specific stoichiometries is generally regarded as disappointing.^{1,2} Research groups have devised kinetic control,^{3–5} controlled etching,^{6,7} and size focusing⁸ schemes to affect nanoparticle size with some success. To this end, several groups have reported kinetic studies that followed gold nanoparticle growth—mainly of thiol-capped MPCs.^{9–21} However, generally, it is believed that the knowledge necessary to synthesize specific gold MPCs must include (1) a series of balanced chemical equations that stepwise build from solution-phase species, through intermediate species of specific composition to form gold MPCs of specific composition, and (2) a set of rate coefficients for these equations that are validated against kinetic data.^{14,21} Knowledge of this reaction mechanism is necessary for implementation of size-selective²² schemes that lead to specific core nuclearities. Thus far, no comprehensive set of chemical reactions that allows for size-selective ligand-capped nanoparticle growth is known; however, data useful for defining this set is emerging.

We published initial explorations of the role of ligand exchange on nascent cluster products²³ and demonstrated that PPh_3 ($PPh_3 =$ triphenylphosphine; Figure 1) can etch gold atoms from PPh_3 -protected nanoclusters.²⁴ More recently, Guidez et al. used density functional calculations to explore the structures and initial growth reactions leading to low-nuclearity gold:phosphine clusters, starting from $Au(PPh_3)Cl$.²⁵ In this work, we report measurements that expand the known reaction mechanism leading to a mixture of diphosphine-protected gold nanoclusters.

Measurements that can identify the reaction mechanisms of MPC growth have proven challenging. Reviews by Watsky, Finney, and Finke describe progress with observations of metallic nanoparticle nucleation and growth.^{26,27} They note that the key barrier to describing growth mechanisms is the absence of methods that identify reaction species and intermediates.²⁷ For example, transmission electron microscopy (TEM), scanning electron microscopy, dynamic light scattering (DLS), and X-ray methods have been used to measure particle growth; however, these methods are insensitive to the solution-phase chemical species that bring about growth. The utility of UV–vis spectroscopy for

Received: May 26, 2011

Published: September 19, 2011

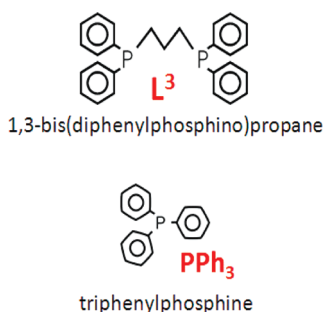


Figure 1. Diphosphine and monophosphine ligands used during this study.

studying gold phosphine complexes and their reactions is well established.²⁸ Although UV–vis spectroscopy offers a sensitive method for monitoring gold nanoparticle growth, other issues may arise, such as the presence of numerous species in the reaction medium that absorb in the UV–vis region and interfere with the nanocluster spectra.²⁹ Moreover, microscopy and UV–vis methods generally do not detect the capping ligands, which are thought to mediate and limit particle growth. More recently, electrospray ionization mass spectrometry (ESI-MS) has emerged as a tool for characterizing nanoclusters.^{3,11,12,23,30–48} A principle advantage of ESI-MS data is that it can establish the stoichiometry of the entire cluster, including the ligand cap.

We recently developed a colorimetric assay that transforms specific groups of PPh₃-protected nanoclusters into two distinct species that can be easily monitored.²⁴ The assay is developed on the basis of known reactions for PPh₃-protected clusters. Addition of the assay reagent, excess L³ (L³ = 1,3-bis(diphenylphosphino)propane), to the solvent system promotes transformation of the cluster distribution with high efficiency. However, little chemical information about the reaction pathways to specific product formation can be derived, and the chemical transformations are specific for PPh₃-containing nanoclusters. Instead, a snapshot of the relative concentrations of the two size bins of different PPh₃-protected clusters can be temporally monitored. Understanding the specific reactions utilized in the assay is important to the overall mechanism of nanocluster formation, but it only comprises a minor portion of the overall reaction mechanism.

Formation of complexes through ligand exchange of diphosphine ligands and Au(PPh₃)Cl prior to reduction yields nanoclusters of remarkable monodispersity.^{22,33} In contrast, reduction of solutions containing only Au(PPh₃)Cl produces a wide distribution of Au_x, 6 ≤ x ≈ 21, clusters.³³ These distinct outcomes demonstrate that diphosphine ligands react along a unique reaction set that forms clusters of monodisperse metal nuclearity. Identification of the active reactions would guide synthesis development. Moreover, the propensity of the Au:L³ reaction system to produce narrow product distributions creates an attractive test system to identify (partially) the reaction mechanism, because it reduces the number of reaction intermediates to a tractable set. Thus, Au:Lⁿ reaction mechanisms are ideal systems for exploration.

For the present study, we collected UV–vis and ESI-MS measurements synchronously in order to follow the product evolution of L³-protected gold nanoclusters. We optimize the reaction conditions to illuminate the largest fraction of the active reaction mechanism. We augment these data with DLS and physical observations. We use polyhedral skeletal electron pair (PSEP) theory to help account for the reaction intermediates and products.

We believe elucidation of formation pathways of different products will allow development of tunable syntheses for different nuclearity clusters, resulting in the ability to examine and characterize cluster properties as a function of nuclearity and ligand cap.

EXPERIMENTAL METHODS

Unless otherwise indicated, all experiments were conducted at ambient temperature ($T = 21–24$ °C) in 1:1 methanol:chloroform solvent systems under argon. Chemicals and solvents were purchased from Sigma-Aldrich and used as delivered.⁴⁹

Synthesis solutions, containing Au(PPh₃)Cl (99.9+ %), L³ (≥97%), and solvent, were prepared in 20 mL borosilicate crimp-sealed vials, sealed by a septum cap with argon in their head spaces, and stirred with a magnetic stirbar for at least 24 h. (Vial components and stirbars are not reused.) Prior to sealing, the stirred solution of ligand complexes was allowed to equilibrate (~15 min)⁵⁰ and argon was bubbled through the solution and passed through a loosely fitted septum. Following equilibration, dry reducing agent, either borane *tert*-butylamine complex (BTBC, 97% pure, (CH₃)₃CNH₂·BH₃) or sodium borohydride (NaBH₄, 98% pure), was quickly added, the solution was again purged with argon, and the vial was crimp sealed. During these last operations the solution was briefly stagnant. To minimize introduction of oxygen, we used a syringe to remove samples through the septum. In the text we refer to solutions prepared with this procedure as “deaerated”. By necessity of apparatus we conducted some experiments with solutions exposed to ambient air. We refer to such solutions as “aerated”.

For all experiments the solutions initially contained [Au(PPh₃)Cl] = (4–10) × 10^{−3} mol·L^{−1}. Ratios of the precursor, ligand, and reducing agent were optimized to obtain the highest total ion current (TIC) in the ESI-MS and to effect efficient reduction of Au^I MPCs (where the superscript of Au^I and Au⁰ denote the atomic oxidation state), while minimizing byproducts originating from reactions between the reducing agent and solvent. These optimum ratios are 1:1:5, respectively, as determined through measurements. Section I of the Supporting Information describes experimental procedures for determining the maximum amount of NaBH₄ that can be added to the solution before interfering artifacts from Na and −(OCH₃) addition⁵¹ and NaB(OCH₃)₄ polymerization appear in the ESI-MS.

Prior knowledge of the reaction mechanism and rate coefficient of NaBH₄ with methanol allows us to define the interval during which electrochemical reduction is important. Sodium borohydride reduces methanol, ultimately producing hydrogen gas (evidenced by bubbles) and sodium tetramethoxyborate via the net reaction



At 273 K the reaction occurs rapidly with a first-order rate constant of $k_1^{273} = 5.8 \times 10^{-4} \text{ s}^{-1}$;⁵² this represents a 20 min half-life. At the average temperature of the present experiments, 296 K, the reducing potential of 1:1 methanol:chloroform solutions may exist for 1 h or so before depletion.

In competition with reaction 1 are the reduction reactions with transition metal complexes, e.g.



where L, L' = PPh₃, L³. Putatively, the electron is transferred during the brief existence of a tertiary or quaternary transition state complex formed by the boronate species and [Au^ILL']⁺. Previous work has described [AuL₂]⁺ as more resistant to reduction,²³ but direct evidence of complexation is not currently described.

Reaction 1 produces intermediate poly methoxyborate anions (e.g., [H₂B(OCH₃)₂][−], [B(OCH₃)₄][−], etc.), which, like [BH₄][−], may also drive reduction reactions. This is known because reaction rate 2, k_2^{borate} ,

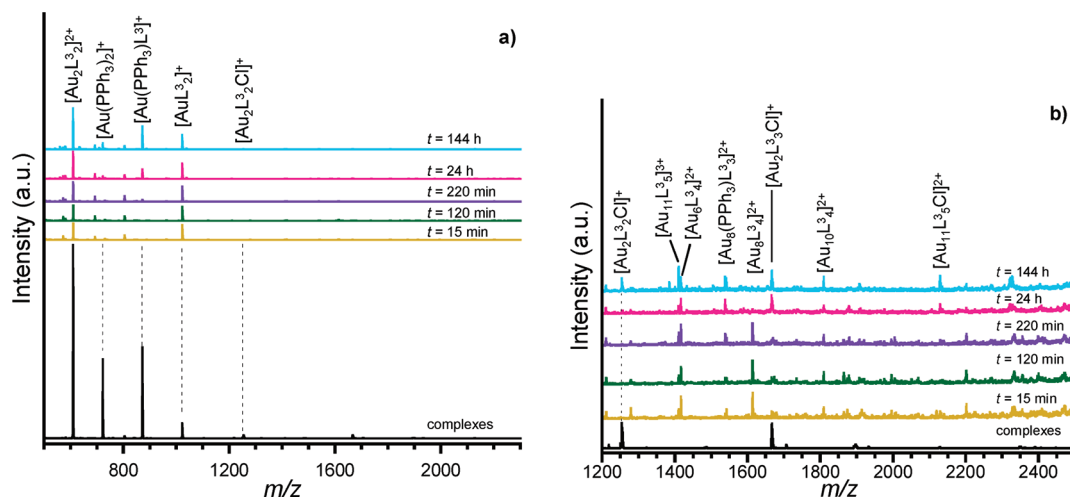


Figure 2. Timed data observed in a deaerated, stirred, 1:1 methanol:chloroform synthesis solution containing $\text{Au}(\text{PPh}_3)\text{Cl}$, L^3 , and NaBH_4 reducing agent, which is added at $t = 0$ min: (a) ESI-MS data observed between 500 and 2300 m/z and (b) ESI-MS data observed between 1200 and 2500 m/z . ESI-MS data in panel a are normalized to exhibit constant $[\text{AuL}_2]^+$ peak intensity, as this species appears inert with respect to reduction. In panel b the ion intensities of each trace are expanded 10 \times , as compared with its corresponding trace in panel a.

changes with alcohol stoichiometry.^{24,53} Thus, each elementary rate coefficient, k_2^{borate} , is specific to a designated boronate species and reaction complex. The action of reaction 2 further shortens the interval during which the solution can reduce chemical species. By employing two reducing agents with different reduction rates but similar reduction potential, we are able to elucidate different reactions occurring in the reaction mechanism.

ESI-MS data were obtained in negative and positive ion modes. ESI-MS comprised an electrospray ion source (Analytica of Branford)⁴⁹ that is coupled to an Extrel CMS quadrupole mass spectrometer (mass range ≈ 10 –3000 m/z). Samples were introduced to the ESI source via direct infusion (10 $\mu\text{L}/\text{min}$) through a glass capillary. Between samples the source was purged with ≥ 1.0 mL of methanol. Stable ion currents were achieved with the potential difference between the capillary exit and the cone voltage set to 80 V.⁵⁴ To ensure data quality and consistency, additional spectra were systematically collected for cone voltages between 60 and 140 V.

This study relies on ESI-MS to identify ionic reactants and products of specific stoichiometry; thus, the ion yield efficiency available from the electrospray environment is critical. In a recent review Di Marco and Bombi⁵⁵ report that comparisons of metal–ligand equilibrium measurements among ESI-MS and other techniques (e.g., NMR, UV–vis, IR) are qualitatively satisfactory; that is, methods generally agree on the composition and relative abundance of observed metal–ligand species. However, for studies designed to obtain quantitative (exact) species concentrations, only fair to poor accord is found. Conductivity and ESI-MS studies have established that stable, ligand-protected gold species containing Au_x ($x = 1$ –13) carry +1 to +3 electrolytic charges.^{22,39,56–73} For such species the ion evaporation model (IEM) for ESI, as explained by Kebarle^{74–77} and Cole,⁷⁸ describes ion formation in the ESI source. Species conforming to the IEM allow examination of suppression effects by recording a series of ESI-MS data for increasing analyte dilutions. When the spectra among the greater dilutions become consistent, the observed spectrum contains minimal ion suppression.^{79,80} During the present study samples drawn from synthesis solutions were diluted to 10^{-4} – 10^{-8} M electrolytes with methanol. In timed experiments samples were analyzed by ESI-MS (or UV–vis) within ~ 5 min of their dilution.

UV–vis spectra were collected on a Varian Cary II dual beam spectrometer.⁴⁹ A set of reference spectra for phosphine-protected Au_x , $8 \leq x \leq 13$, are presented in the Supporting Information. Sedimentation studies of colloid solutions were conducted using a Beckman-Coulter

Optima MAX-XP ultracentrifuge. Dynamic light scattering (DLS) measurements of colloids were conducted using a Malvern Zetasizer Nano ZS equipped with a 4 mW 633 nm (He–Ne) laser. Section II of the Supporting Information provides details regarding these measurements.

RESULTS

1. Au_xL^3 Cluster Growth in Deaerated Methanolic Solutions via Reduction by NaBH_4 . Experimental results shown in this section summarize the ESI-MS and UV–vis measurements of deaerated, stirred, equilibrated, 1:1 methanol:chloroform synthesis solutions as they respond to reduction by NaBH_4 . In Figure 2a and 2b the traces labeled “complexes” show the ion spectra obtained from dissolution and equilibration of equimolar $\text{Au}(\text{PPh}_3)\text{Cl}$ and L^3 . The most intense ion peaks are $[\text{Au}_2\text{L}_3]^{2+}$, $[\text{Au}(\text{PPh}_3)_2]^+$, $[\text{Au}(\text{PPh}_3)\text{L}_3]^+$, and $[\text{AuL}_2]^+$ and trace abundances of $[\text{Au}_2\text{L}_3\text{Cl}]^+$ and $[\text{Au}_2\text{L}_3\text{Cl}]^+$. Unreduced solutions of Au^{I} complexes appear clear and colorless.

Reduction was initiated (thus, defining $t = 0$ min) by adding 5 \times molar excess of solid NaBH_4 into the pre-equilibrated synthesis solution. Immediately, the solution became turbid, exhibiting a dark brown-black color. At $t = 15$ min (Figure 2), the ESI-MS data revealed that ion currents from $[\text{Au}(\text{PPh}_3)_2]^+$, $[\text{Au}(\text{PPh}_3)\text{L}_3]^+$, $[\text{Au}_2\text{L}_3\text{Cl}]^+$, and $[\text{AuL}_2]^+$ were depleted and that $[\text{Au}_2\text{L}_3]^{2+}$ ion current was diminished by $\sim 20\times$.⁵⁴ In contrast, the intensity of the $[\text{AuL}_2]^+$ peak appeared unchanged. In the ESI-MS spectrum rapid depletion of the ion peaks of Au^{I} complexes is evidence that electrochemical reduction produces a solution containing Au^0 complexes predominately. These complexes react among themselves and with cations, forming cationic complexes of higher gold nuclearity that appear above 1400 m/z (Figure 2b). ESI-MS data collected in negative ion mode in unreduced and reduced solutions exhibited only Cl^- .

We note that 15 min after NaBH_4 is added to the equilibrated solution ion peaks appear between 1400 and 2500 m/z . These new products are assigned to $[\text{Au}_6\text{L}_3]^{2+}$, $[\text{Au}_8(\text{PPh}_3)\text{L}_3]^{2+}$, $[\text{Au}_8\text{L}_4]^{2+}$, $[\text{Au}_{10}\text{L}_4]^{2+}$, and $[\text{Au}_{11}\text{L}_5]^{3+}$ (Figure 2b). By $t = 120$ min, the reduction potential of the solution is essentially depleted⁵² yet ion peak intensities continue to change, providing

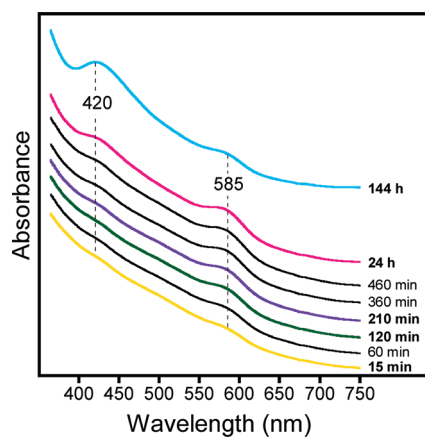


Figure 3. Timed UV–vis spectra observed for the same stirred, deaerated 1:1 methanol:chloroform synthesis solution, as shown in Figure 2. The solution contains Au(PPh₃)Cl, L³, and NaBH₄. The reducing agent was added at $t = 0$ min.

evidence for the activity of other chemical processes. For example, the [Au₈L₃₄]²⁺ peak, which appeared at $t = 15$ min, is depleted by $t = 24$ h. We also note that by $t = 144$ h (6 days) the [Au₁₁L₃₅Cl]²⁺ and [Au₁₁L₃₅]³⁺ peaks have grown in intensity but the [Au₆L₃₄]²⁺ peak has not increased.

The timed UV–vis spectra (Figure 3) poll the combined abundances of the ionic and neutral ensembles of phosphine-protected gold cores of the set {Au_{*x*}: 6 ≤ *x* ≤ 13}. Initially, the band centered at 585 nm rapidly grows, but by $t = 460$ min (~7.7 h) its growth has ceased. The 585 nm absorption band and corresponding m/z 1416 peak present in the ESI-MS data (Figure 2) are characteristic of [Au₆L₃₄]²⁺.²⁴ A second band centered at 420 nm grows during the entire 144 h (6 day) duration of these experiments. Comparisons of these absorption profiles with reference spectra verify that the 420 nm band comprises contributions from members of the phosphine-ligated set {Au_{*x*}: 8 ≤ *x* ≤ 12}.²² The absorption coefficients of these bands are not known; thus, the observed absorptions only indicate the population changes over time.

Interpretation of the 585 nm absorption band behavior is not straightforward. Previous studies have established that L³ ligands completely replace PPh₃ on the surface of ligated Au₈ and Au₉ clusters, irrespective of charge, to form [Au₆L₃₄]²⁺.^{24,81,82} Since the present reaction system contains an abundance of L³ ligands, the 585 nm absorption of [Au₆L₄]²⁺ is proportional to the nascent PPh₃-ligated Au₈ and Au₉ clusters; therefore, the 585 nm absorption band indicates that PPh₃-protected Au₈ and Au₉ clusters are synthesized during the reduction interval (~80 min) and that the set continues to gain population through $t \approx 7.7$ h. Formation of significant populations of the ligated Au₈ and Au₉ clusters produced from the fast NaBH₄ reduction of phosphine-containing complexes is consistent with our observations during reduction of the AuClPPh₃ precursor only.²⁴ [Au₆L₃₄]²⁺ is not predicted to be available to reactions that increase gold core nuclearity (vide infra). However, in the absence of excess amounts of L³, conversion of PPh₃-containing Au₈ and Au₉ clusters into [Au₆L₃₄]²⁺ is incomplete, resulting in a residual population of PPh₃ containing clusters.

Interpretation of the 420 nm absorption band is similarly complex. Growth of the 420 nm band indicates that source reactions are producing the PPh₃- and L³-ligated Au_{*x*}, $x \leq 8$; yet

growth of the 585 nm band tells us that the 420 nm band is diminished because a fraction of the nascent Au₈ and Au₉ products is depleted by production of [Au₆L₄]²⁺. Therefore, the 420 nm absorption band comprises mostly ligated clusters of the set {Au_{*x*}: 10 ≤ *x* ≤ 12}.

The UV–vis data (Figure 3) are in accord with the ESI-MS data (Figure 2b). The UV–vis data indicate that ligated, higher nuclearity clusters continue to become more abundant for several days after the initial reduction period. Similarly, between $t = 24$ and 144 h [Au₁₀L₃₄]²⁺, [Au₁₁L₃₅]³⁺, and [Au₁₁L₃₅Cl]²⁺ peaks become more prominent in the ESI-MS. Interestingly, comparison of the integrated areas of two UV–vis absorption bands to the relative signal intensities from [Au₆L₃₄]²⁺ and ligated Au₁₀ and Au₁₁ clusters in the ESI-MS spectra produces a constant molar absorptivity ratio, $\epsilon_{585}/\epsilon_{420}$, from 15 min to 24 h. The trend is broken at 144 h, where large broadening on the red side of the $\lambda_{\max} = 420$ nm is observed, suggesting ligated Au₁₀ and Au₁₁ populations can be initially surveyed with ESI-MS and UV–vis. The authors acknowledge competing effects during this time frame may exist to compensate for the relationship of $\epsilon_{585}/\epsilon_{420}$.

On the basis of the UV–vis and ESI-MS data, we interpret the continuous growth of the 420 nm absorption band as evidence that the set {[Au_{*n*}(PPh₃)_{*w*}L_{*x*}_{*y*}]^{*z+*}: 8 ≤ *n* ≤ 12}, increases population through $t = 144$ h. Since this growth continues long after the reduction interval (~80 min), growth must partially arise from the etching of nanoparticles of higher gold nuclearity, i.e., Au_{*x*}, $x \geq 13$. The ESI-MS and UV–vis data do not support an alternate mechanism involving growth from clusters of lower metal nuclearity, i.e., Au_{*x*}, 1 ≤ *x* ≤ 7. The initial growth of the 585 nm band shows that [Au_{*x*}(PPh₃)]^{*z+*}: 8 ≤ *x* ≤ 9, exist in solution through $t = 24$ h, either through nascent production during the reduction interval or through etching of PPh₃-containing clusters of higher nuclearity.

Growth of Au_{*x*}, $x \geq 10$, clusters also correlates with a color change. After 6 days the solution color has changed from brown-black to a dark black-gray. An orange cast, characteristic of phosphine-ligated Au₁₀ and Au₁₁ clusters, is observed in the solution meniscus.

2. Au_{*x*}L³ Cluster Growth in Deaerated Solutions through Reduction by BTBC. BTBC reacts more slowly than NaBH₄ with Au^I complexes, as reflected in the rate of diminishing ion current in the ESI-MS data. This unknown slower reaction rate also extends the duration of reduction potency in solution, which theory predicts²⁶ and experiment²⁴ has determined can produce different distributions of metal nuclearities. Figure 4 shows ESI-MS measurements over 77 days of deaerated, stirred, 1:1 methanol:chloroform synthesis solutions containing equimolar ratios of Au(PPh₃)Cl and L³, as they respond to reduction by 5 × molar BTBC. Figure S5, Supporting Information, shows corresponding ESI-MS data for deaerated, stirred, neat chloroform synthesis solutions.

For both solutions the Au(PPh₃)Cl and L³ solutes were allowed to dissolve and achieve equilibration, as measured by ESI-MS. Addition of solid BTBC to the equilibrated solution induced the solution to become turbid and dark brown-black in color, consistent with formation of colloidal gold species (vide infra). Again, ESI-MS data collected in negative ion mode for unreduced and reduced solutions exhibited only Cl⁻.

Almost immediately after addition of BTBC to the 1:1 methanol:chloroform solution ($t \approx 5$ min), the ESI-MS data exhibits prominent signal from [Au₈(PPh₃)₃L₃]²⁺, [Au₈(PPh₃)₂L₃]²⁺, and [Au₉(PPh₃)L₃Cl]²⁺ (Figure 4a). By $t = 77$ h the abundances

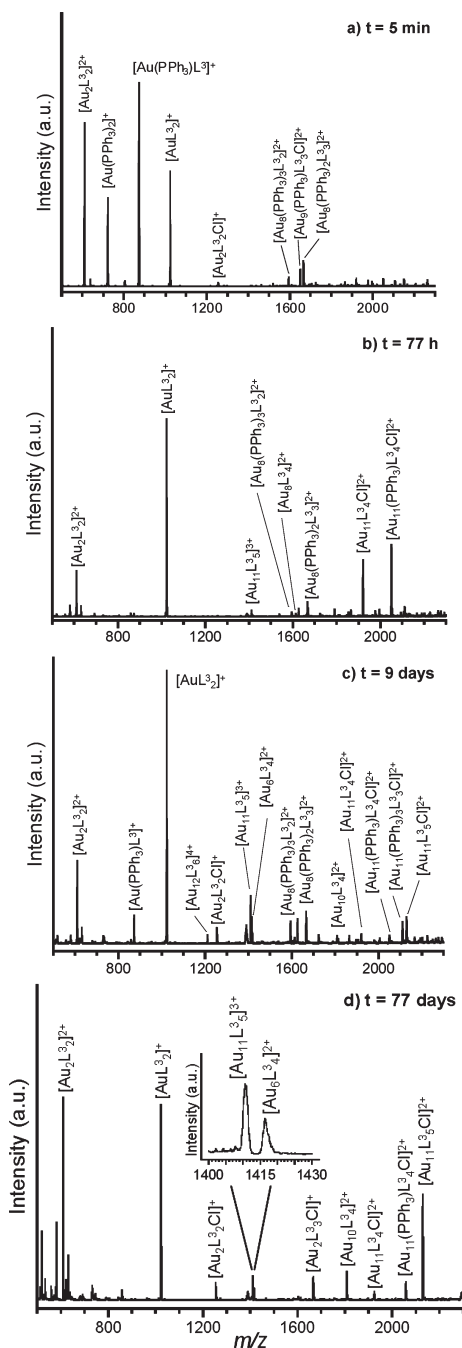


Figure 4. ESI-MS data from a stirred, deaerated 1:1 methanol:chloroform solution of Au(PPh₃)Cl, L³, and BTBC prepared in a 1:1:5 molar ratio, observed at reaction times (a) $t \approx 5$ min, (b) $t = 77$ h, (c) $t = 9$ days, and (d) $t = 77$ days. (Inset) Enlarged view of the [Au₁₁L₃]³⁺ and [Au₆L₃]⁴⁺ ion peaks.

of [Au(PPh₃)₂]⁺ and [Au(PPh₃)L³]⁺ are greatly diminished but [AuL₃]²⁺ remains prominent (Figure 4b). Ion signals from higher nuclearity clusters also include [Au₈(PPh₃)₂L₃]²⁺, [Au₈(PPh₃)₃L₃]²⁺, [Au₈L₃]²⁺, [Au₁₁L₃]³⁺, [Au₁₁L₃Cl]²⁺, and [Au₁₁(PPh₃)L₃Cl]²⁺.

At $t = 9$ days (Figure 4c) the 1:1 methanol:chloroform solution continues to display signals from [Au₈(PPh₃)₃L₃]²⁺, [Au₈(PPh₃)₂L₃]²⁺, [Au₁₁L₃]³⁺, [Au₁₁L₃Cl]²⁺, and [Au₁₁(PPh₃)L₃Cl]²⁺. This set is augmented by newly emergent ESI-MS

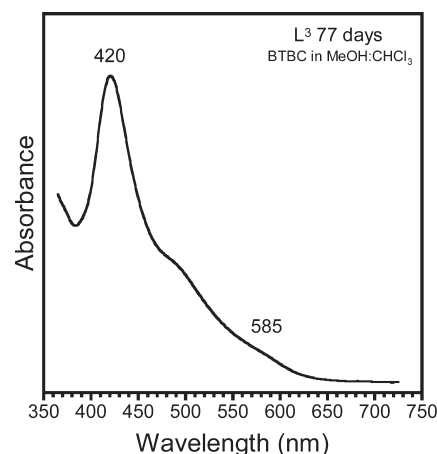


Figure 5. UV-vis data observed after preparation of a stirred, deaerated 1:1 methanol:chloroform synthesis solution containing L³, Au(PPh₃)Cl, and BTBC reducing agent; UV-vis observed at $t = 77$ days.

peaks from [Au₆L₃]⁴⁺, [Au₁₀L₃]²⁺, [Au₁₁(PPh₃)₃L₃Cl]²⁺, [Au₁₁L₃Cl]²⁺, and [Au₁₂(-L³)L₃]⁴⁺, where -L³ denotes putative, monodentate complexation. (Since Au₁₂ cores have only 11 available sites for complexation, a monodentate ligand is stipulated.) The weak [Au₈L₃]²⁺ peak is now depleted. Reductions conducted in neat chloroform solution display similar data; however, after $t = 9$ days the ion signals (Figure S5, Supporting Information) cease to change perceptibly.

Finally, at $t = 77$ days (Figure 4d) signals from [Au₆L₃]⁴⁺, [Au₁₀L₃]²⁺, [Au₁₁L₃]³⁺, [Au₁₁L₃Cl]²⁺, [Au₁₁L₃Cl]²⁺, [Au₁₁(PPh₃)L₃Cl]²⁺, and [Au₁₁L₃Cl]²⁺ remain apparent. Ligated Au₈ cations are depleted. Signal from [AuL₃]²⁺ remains abundant. The UV-vis spectrum of the $t = 77$ days solution (Figure 5) exhibits a prominent 420 nm band, corresponding to λ_{\max} of ligated Au₁₀ and Au₁₁ clusters, and the extended red-shifted absorption tail reflects the broad absorption band of [Au₆L₃]⁴⁺, which has $\lambda_{\max} = 585$ nm.

Over the interval of this study with BTBC the solution color changed from black-orange. An orange cast is observed in the solution meniscus, which is in accord with the presence of phosphine-ligated Au₁₀ and Au₁₁ clusters. The visual appearance of the solution is similar to the synthesis solution reduced by NaBH₄.

3. Cluster Formation and Agglomerate Characterization in Aerated solutions. The deaerated solutions exhibit colorations consistent with the presence of [Au₆L₃]⁴⁺ and [Au₁₁L₃]³⁺, and an overall dark appearance remains, consistent with the presence of colloids. Further studies characterized the colloid. Since the deaerated solutions have an opportunity to be exposed briefly to ambient conditions, additional UV-vis and ESI-MS data for aerated solutions were collected to examine the role of dissolved oxygen.

At early times ($t < 8$ h) aerated and deaerated solutions appear visually and chemically similar with only small changes in the complex distribution visible prior to reduction. When an aerated, freshly prepared 1:1 methanol:chloroform solution of NaBH₄ is poured into a like solution that contains equimolar Au(PPh₃)Cl and L³, the solution develops a turbid, dark brown—almost black—appearance within seconds (Figure S2a, Supporting Information), suggesting formation of colloidal species. Just as observed for deaerated solutions, the aerated solutions (Figure 6a)

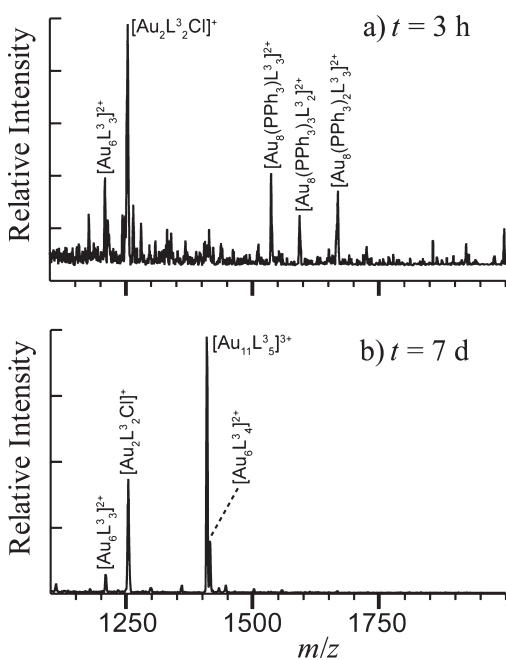


Figure 6. ESI-MS data observed at reaction times following preparation of a stirred, aerated, 1:1 methanol:chloroform synthesis solution containing Au(PPh₃)Cl, L³, and BTBC reducing agent. Panels depict data for reaction times (a) $t = 3$ h and (b) $t = 7$ days.

first exhibit [Au₈(PPh₃)L₃]²⁺, [Au₈(PPh₃)₂L₃]²⁺, and [Au₈(PPh₃)₃L₂]²⁺. Thus, we conclude that ambient oxygen does not greatly perturb solutions at early times. Interestingly, at $t = 60$ days this solution exhibits larger nuclearity clusters, [Au₁₂L₃Cl]³⁺ and [Au₁₃L₃Cl₂]³⁺, in the aerated ESI-MS, indicating their lower relative reactivity with oxygen (Figure S6, Supporting Information).

The similarity between aerated and deaerated solutions allows us to conduct sedimentation and dynamic light scattering experiments on freshly prepared solutions. Each experiment was completed within 90 min. These experiments reveal that the black color originates from hydrophobic colloids of agglomerated primary clusters (defined as ([Au_nL_xL'_y]^{z+}),_n where n is large, and L, L' = PPh₃, L³). In accord with the IUPAC definition of agglomeration, which stipulates weak, reversible interactions between primary clusters,⁸³ experiments ascertained that the primary clusters comprising the colloid remain available for resorption to solution. (Similar reversible processing of agglomerates is observed during our previous study of PPh₃-protected MPCs.)²⁴ Hence, within a reaction mechanism agglomerates mainly act as primary cluster reservoirs that should affect mass transport rates. Ligand exchange to fully L³-protected MPCs promotes the reversible processing of colloids, providing evidence that the primary L³-protected clusters are more stable in solution than their PPh₃-protected counterparts. Further discussion of the measurements is found in section II of the Supporting Information. Further exploration of the colloid is beyond the scope of this report.

As time progresses beyond $t = 3$ h, the aerated solution begins to differ from the deaerated solutions. For example, at $t = 7$ days, the aerated solutions only exhibit product signal from [Au₆L₃]²⁺ and [Au₁₁L₅]³⁺ (Figure 6b). Absent from these aerated ESI-MS data are chlorinated cationic clusters (Figure 4). Qualitatively, the total ion current of the aerated ESI-MS is lower than that observed in the deaerated ESI-MS, indicating a lower product yield of the cationic clusters. The UV-vis spectrum of the

solution at $t = 7$ days (not shown) contains two absorption bands centered at 420 and 585 nm consistent with the ESI-MS data. In contrast to the deaerated systems, the visual appearance of the solution at $t = 20$ days is a bright orange (Figure S2b, Supporting Information) and has lost all of the dark visual appearance initially present after BTBC addition (Figure S2a, Supporting Information). The corresponding UV-vis spectrum of this orange solution (not shown) contains a single λ_{max} centered at 420 nm corresponding to [Au₁₁L₅]³⁺.

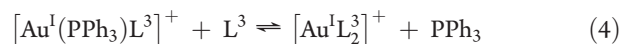
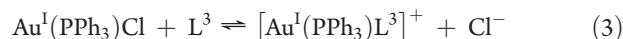
DISCUSSION

As observed in the UV-vis spectra and ESI-MS data, formation of gold MPCs proceeds via two stages. The first stage comprises reduction of the ligated Au^I complexes, which produces a high concentration of ligated Au⁰ free radicals. These free radicals react forming a distribution of clusters. This result is in accord with theory²⁶ and previous experiments²⁴ showing that the kinetic rate of the reducing agent can govern the initial distribution of cores. During the second stage, chemical processing of nanoclusters by solution-phase chemistry can change the size distribution of the sample. Such postreduction processing can lead to the predominance of one or two nuclearities. Use of two reducing agents with different reducing rates allows us to examine distinct stages with NaBH₄ and overlapping processing of the two stages in the BTBC systems.

The present UV-vis and ESI-MS data evidence numerous cluster stoichiometries among the nascent, intermediate, and final gold MPCs. In the following sections we present reactions that account for these species. By identifying the many elementary reactions, the reaction mechanism is defined and populated by a set of coarsely defined elementary rate coefficients, e.g., k_i ; has a significant rate coefficient or k_i is null.

1. Ligand-Exchange-Induced Dissolution of Au^I(PPh₃)Cl.

During the equilibration process that precedes reduction, dissolution of the starting material, Au^I(PPh₃)Cl, produces a distribution of ionic and neutral complexes in the synthesis solutions. As we recently demonstrated with ESI-MS measurements, the dissolution process of Au(PPh₃)Cl in a stoichiometric excess of phosphine ligands includes the following reactions²³



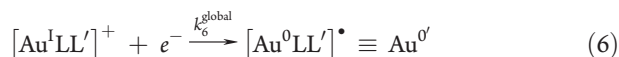
Other complexes, such as [Au_xL_x]^{x+} and [Au₂L₂Cl]⁺, are also among the dissolution products (Figure 2a). These species are reported to be stabilized by bridging L³ ligands.⁵⁷ We do not list other ternary and quaternary complexes of phosphine-ligated Au^I, which may also be present at equilibrium.

The majority of the dissolution products contains two-coordinate gold-phosphine complexation. The preference by Au^I to form two-coordinate linear complexes exists because the linear [Au^I(PPh₃)₂]⁺ orbital manifold is split into seven orbitals (sp^d⁵) at lower energy and two high-lying p orbitals.⁸⁴ Thus, two-coordinate linear complexes of Au^I that contain 14 valence electrons comprise a highly stable, closed-shell configuration.⁸⁵ Relativistic ab initio calculations of [Au^I(PH₃)_n]⁺ ($n = 1-4$) and Au^I(PH₃)_nCl ($n = 1-3$) complexes also find that Au^I strongly favors the coordination number of two; hence, [Au^I(PH₃)₂]⁺

and $\text{Au}^{\text{I}}(\text{PH}_3)\text{Cl}$ are the most stable species in these series, which is enhanced by strong relativistic effects.⁸⁶ This effect also applies to PPh_3 and L^3 ligands, which coordinate with gold more strongly than PH_3 .^{25,87,88}

2. Reduction of $[\text{Au}^{\text{I}}\text{LL}'^3]^+$ Species To Form $\text{Au}^{0'}$ Species.

The observation that adding NaBH_4 to the synthesis solution rapidly depletes mono- and digold complex signals is direct evidence that methanolic solutions at $t \approx 1$ h (when most reduction potential has been consumed) contain predominantly neutral species (Figure 2). Solution-phase reduction is symbolized as

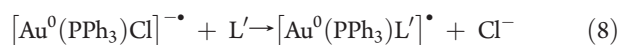


where $\text{L}, \text{L}' = \text{PPh}_3, \text{L}^3$. The added electron resides in the singly occupied $\text{hy}(s-z)$ orbital (that contains some $6s$ density) of the $\text{Au}^{0'}\text{LL}'^3$ free radical.⁸⁷ For simplicity, we define $\text{Au}^{0'}$ to denote a generalized $[\text{Au}^{0'}\text{LL}'^3]^\bullet$ free radical, so that we may present subsequent reactions without explicitly accounting for the ligands on the gold reactants and products. The electron is donated by the borane reducing agent, BTBC or NaBH_4 , or their chemical derivatives (such as $[\text{BH}_2(\text{CH}_3\text{O})^-]$),^{52,89,90} and k_6^{global} is the global reduction rate coefficient of the specified gold species for all elementary rate coefficients, k_2^{borate} (reaction 2). For the present study we can restrict the set of reducing agents to borate species. Previous work on the reduction of comparable Au^{I} complexes in solution has found that the alcohol radical manifests insufficient potential to promote formation of $\text{Au}^{0'}$.⁹¹

Synthesis solutions contain the starting reagent, $\text{Au}^{\text{I}}(\text{PPh}_3)\text{Cl}$. Recently Guidez et al.²⁵ used ab initio computational methods to predict the initial growth mechanisms of gold–phosphine clusters that are initiated by the reaction

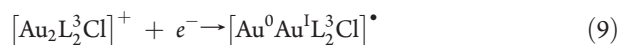


where the added electron density is contained mainly in an orbital of π^* character on the phenyl rings. During the present experiments, Cl^- is the only anion observed. This apparent discord is reconciled if a free phosphine ligand induces ligand exchange with the radical anion, producing $\text{Au}^{0'}$ free radical complex



as observed for $\text{Au}(\text{PPh}_3)\text{Cl}$ in solution (reaction 3).

The ESI-MS data of the present (Figures 2a and 4d) and prior studies²³ show that $[\text{Au}(\text{PPh}_3)_2]^+$ and $[\text{Au}(\text{PPh}_3)\text{L}^3]^+$ are reduced to depletion via reaction 6. The near or complete depletion of ESI-MS signal from the L^3 -bridged $[\text{Au}_2\text{L}^3_2\text{Cl}]^+$ complex (cf. Figures 2 and 4b) is evidence for, at least, the partial reduction reaction

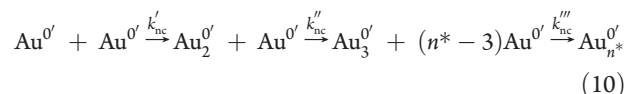


which forms a free radical containing gold in heterogeneous oxidation states. In summary, reduction of solution-phase species produces predominantly the free radicals, $[\text{Au}^0(\text{PPh}_3)_2]^\bullet$, $[\text{Au}^0(\text{PPh}_3)\text{L}^3]^\bullet$, and $[\text{Au}^0\text{Au}^{\text{I}}\text{L}^3_2\text{Cl}]^\bullet$.

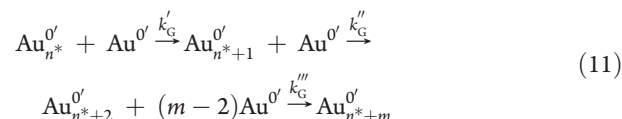
3. Nucleation and Core Growth of $\text{Au}^{0'}$ Species. The presence of a large concentration of free radical complexes, $\text{Au}^{0'}$, such as those generated by reactions 6–9, will favor self-reactions among the nascent and secondary products. Quantitative measurements of unique species could allow adoption of a parameterized method for modeling cluster growth up to the nuclearities detected by the experimental apparatus. For example, the kinetics of the nanocluster formation process could be fitted with the

modified Finke–Watzky 2-step, slow continuous nucleation and core growth mechanism.²⁶ The proposed model involves diffusion-limited processes in both nucleation and core growth.²⁴

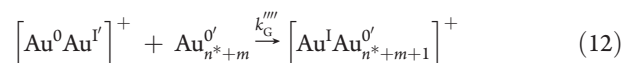
Nucleation:



Diffusion-Limited Core Growth:



and



where $[\text{Au}^0\text{Au}^{\text{I}}]^+$ is a gold cation, and primes indicate ligation. As shown, the model allows for formation of both cations and electrically neutral products, as is consistent with the present observations. Cluster growth data can be fit using two global rate coefficients: k_{nc} , the global nucleation reaction rate coefficient that describes stepwise formation of a critical gold nucleus size of n^* atoms,^{24,26} and k_{G} , the global core growth rate coefficient that describes the stepwise growth of clusters to sizes larger than the critical nucleus size, n^* . In the absence of detailed rate data, these global rate coefficients are approximated by an average rate across the elementary reaction steps (i.e., $k_{\text{nc}} \approx k_{\text{nc}}' \approx k_{\text{nc}}'' \approx k_{\text{nc}}''' \approx \dots$; $k_{\text{G}} \approx k_{\text{G}}' \approx k_{\text{G}}'' \approx k_{\text{G}}''' \approx \dots$) and k_{nc} may contain contributions from k_6^{global} , however, all simplifications can be replaced with explicit rate coefficients as more detailed kinetics data become available.²⁶

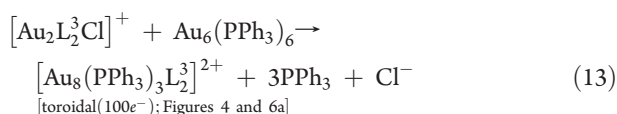
Evans and Mingos analyzed the (in vacuo) species $[\text{Au}(\text{PPh}_3)_n]^{z+}$ ($2 \leq n \leq 6$), concluding that the $\text{hy}(s-z)$ orbital of the $\text{Au}(\text{PPh}_3)$ fragment accounts for much of the bonding.⁸⁷ Within this orbital analysis they note that the $\text{Au}(\text{PPh}_3)$ fragment is isolobal⁹² to $[\text{Au}^0(\text{PPh}_3)_2]^\bullet$.^{28,87,88} In view of this isolobal relationship, low-energy barriers for condensation reactions between $[\text{Au}^0(\text{PPh}_3)_2]^\bullet$ and $[\text{Au}_n(\text{PPh}_3)_n]^{z+}$ ($n < 12$) should exist, where the transition state complex subsequently eliminates a PPh_3 ligand. Thus, these considerations can account for the activity of free radical reactions 10 and 11. However, the relative lack of selectivity and monodispersity observed in recent PPh_3 -protected nanocluster studies^{24,33} supports increased efficacy for diphosphine ligands to control both reduction and subsequent solution-phase processing reactions.²²

4. Formation of Au_x Ligand Cations through Neutral-Ion Reactions. The UV–vis absorption bands and ESI-MS data observed in solutions reduced by NaBH_4 provide evidence that substantial populations of neutral MPCs are rapidly produced. The ESI-MS data show that reduction by NaBH_4 depletes nearly all ion signals from complexes, while concomitantly the UV–vis spectra exhibit cluster growth. Ion cluster signals from larger ligated Au_x , $8 \leq x \leq 13$, MPCs eventually grow into the ESI-MS data over time, evidencing the activity of ion-neutral reactions. The observed ionic cluster can be accounted by using simple electron counting schemes.

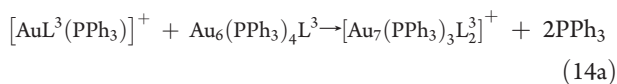
PSEP analysis, as developed by Mingos and others,^{28,93–96} may be applied to predict the most stable core geometry for ligated, closed-shell gold clusters of the form $[\text{Au}\{\text{Au}(\text{PPh}_3)\}_n]^{z+}$

comprising a central Au surrounded by n_s peripheral Au–PR₃ fragments. Especially stable gold atom configurations have the peripheral Au atoms arranged to form (1) spherical polyhedral clusters characterized by a total of $12n_s + 18$ valence electrons or (2) toroidal (or elliptical) polyhedral clusters characterized by a total of $12n_s + 16$ valence electrons.^{85,97} For gold–phosphine Au_x ($x = 8–13$) MPCs good accord exists between the solid state structure determined from X-ray crystallography data and the gold atom arrangement predicted from PSEP analysis.^{39,56–73}

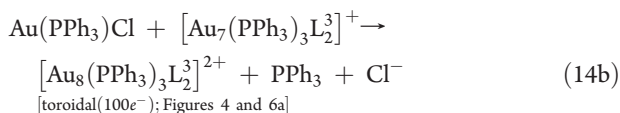
Growth of higher metal nuclearity Au_x cations, as observed in the ESI-MS data, is evidence that neutral clusters react with Au^I-containing species to form stable ionic clusters. Solutions reduced by either NaBH₄ or BTBC exhibit ligated Au₈ cations containing two or more L³ ligands. A variety of reaction schemes can account for the transfer of a cluster from the neutral to cationic ensembles, e.g.



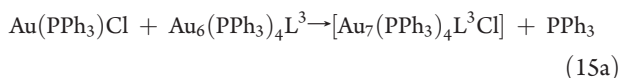
or



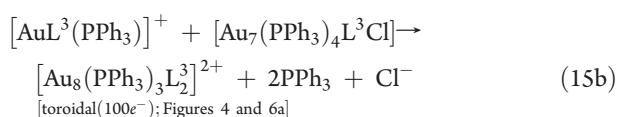
and



or



and



Reaction 14a prepares $[\text{Au}_7(\text{PPh}_3)_3\text{L}_2^3]^+$, which is similar to the characterized $[\text{Au}_7(\text{PPh}_3)_7]^+$ and likely contains no central atom and has its Au atoms arranged approximately in a pentagonal bipyramidal geometry.⁶⁴ Reaction 15a creates a similar neutral complex. In reactions 14b and 15b these Au₇ species react with Au^I(PPh₃)Cl to form ligated Au₈ species. We expect both reactions to proceed rapidly, as acquisition of a central gold atom reinforces radial bonding in Au₈ and larger clusters.^{28,95,98}

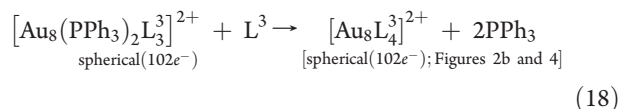
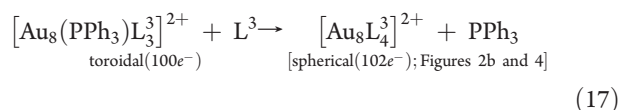
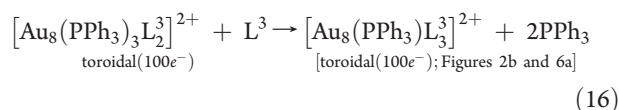
The existence of these reactions is supported by observation of core expansion reactions involving $[\text{Au}_7(\text{PPh}_3)_7]^+$.^{64,99} Reactions 14a, 14b, 15a, and 15b may involve a variety of ligated Au₇ species reactants, and this variety can account for the observed early products: $[\text{Au}_8(\text{PPh}_3)_2\text{L}_3^3]^{2+}$, $[\text{Au}_8(\text{PPh}_3)\text{L}_3^3]^{2+}$, and $[\text{Au}_8\text{L}_4^3]^{2+}$ (Figures 2b and 4).

Here we comment on the annotations within reactions 13, 14b, and 15b that are a form we use to illustrate the accord between PSEP theory and the ESI-MS data throughout this article. Beneath each observed, closed-shell product cluster an annotation lists the valence electron count; the arrangement of the gold

atoms, as determined by PSEP analysis, and a list of figures that contain the supporting ESI-MS data.

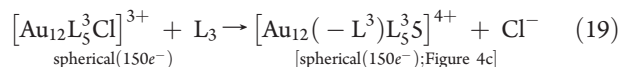
5. Formation of Uniform Ligand Caps. Complexation between Au and L³ is stronger than between Au and PPh₃.²³ Thus, given sufficient L³ in solution, L³ will displace PPh₃ completely. Ligand exchange within this chemical system is ubiquitous, proceeding concomitant with every other chemical reaction. Importantly, ligand exchange is driven by the concentration of free ligands in solution, which, in turn, is strongly coupled to the reduction rate of the phosphine-protected Au^I complexes. Therefore, preferential reduction and condensation of PPh₃-protected complexes results in less liberated L³, which directly affects ligand exchange on nascent nucleation products.

Exchanges of L³ for PPh₃ are observed in the ESI-MS data. For example, ESI-MS data show that signals from $[\text{Au}_8(\text{PPh}_3)\text{L}_3^3]^{2+}$, $[\text{Au}_8(\text{PPh}_3)_2\text{L}_3^3]^{2+}$, and $[\text{Au}_8(\text{PPh}_3)_3\text{L}_2^3]^{2+}$ emerge with or prior to the appearance of $[\text{Au}_8\text{L}_4^3]^{2+}$ (Figures 2, 4, and 6a). This result evidences the activity of ligand exchange reactions among the octagold species, e.g.



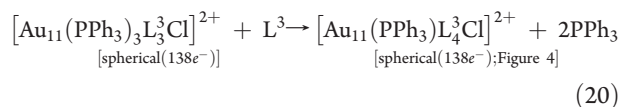
For the bidentate L³ ligand the initial complexation may involve monodentate complexation, e.g., reaction 18 may first form $[\text{Au}_8(\text{PPh}_3)(-\text{L}^3)\text{L}_3^3]^{2+}$ that is followed by an autologous ligand exchange that displaces a second PPh₃ ligand.

Evidence for the existence of stable monodentate bonding by L³ is found in the observation of $[\text{Au}_{12}\text{L}_6^3]^{4+}$. This species may form via

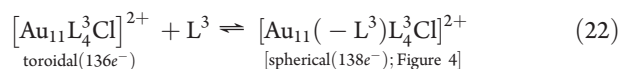
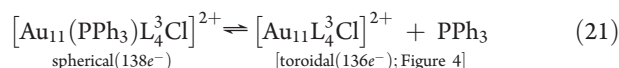


where $-\text{L}^3$ displaces Cl⁻ and engages in monodentate binding with a peripheral Au.

Ligand exchange can account for the loss of $[\text{Au}_{11}(\text{PPh}_3)_3-\text{L}^3\text{Cl}]^{2+}$ during BTBC reductions between $t = 9$ and 77 days

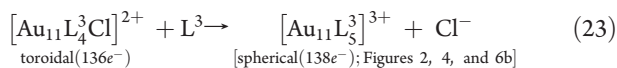


The ESI-MS data suggest that $[\text{Au}_{11}(\text{PPh}_3)\text{L}_4^3\text{Cl}]^{2+}$ is in equilibrium with $[\text{Au}_{11}\text{L}_5^3\text{Cl}]^{2+}$ and with $[\text{Au}_{11}\text{L}_4^3\text{Cl}]^{2+}$ as these species appear together



PSEP analyses indicate that $[\text{Au}_{11}\text{L}_3^3\text{Cl}]^{2+}$ exists as a stable, toroidal cluster with one peripheral Au that is not engaged in complexation. When this site complexes with PPh_3 and L^3 ligands, it forms a stable, spherical cluster; however, the effects of steric hindrance and solvation energy may govern the equilibria indicated in reactions 21 and 22. The cluster $[\text{Au}_{10}\text{L}_3^3]^{2+}$ is also expected to contain an uncomplexed peripheral Au site; however, the present ESI-MS data do not detect the corresponding $[\text{Au}_{11}(\text{PPh}_3)\text{L}_3^3\text{Cl}]^{2+}$ and $[\text{Au}_{11}(-\text{L}^3)\text{L}_3^3\text{Cl}]^{2+}$ signals.

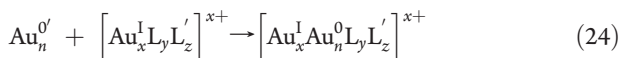
In principle, the ligand exchange reaction



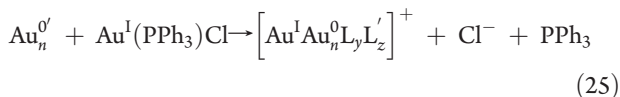
is possible. As indicated, $[\text{Au}_{11}\text{L}_3^3\text{Cl}]^{2+}$ is a stable toroidal cluster with one peripheral Au that does not engage in complexation. The minimum energy reaction path is expected to proceed by forming a stable $[\text{Au}_{11}(-\text{L}^3)\text{L}_3^3\text{Cl}]^{2+}$ spherical (138e⁻) complex.

Ligand exchange reactions analogous to reactions 16 through reaction 23 are available to most gold clusters containing PPh_3 and, at times, Cl^- . Over time and in the presence of free L^3 , the ligand caps of almost all Au_x species will exchange and the ligand caps of the end products will tend to contain the stronger ligand.

6. Postreduction Reactions That Increase Au_x Charge State. At early times processes driven by free radicals (i.e., reactions 9, 10, and 11) dominate product formation. After the reducing potential of the solution is depleted, such reactions essentially cease. However, reactions that change the electrical charge of Au_n^0 clusters may continue. These reactions have the form

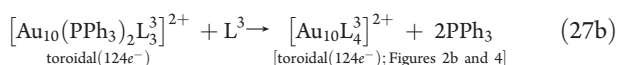
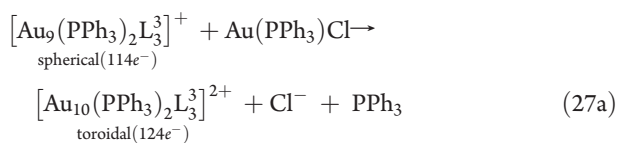
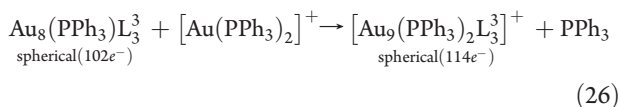


and/or



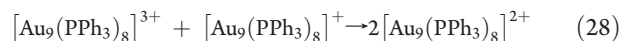
Most likely, reactions 24 and 25 are equally active for clusters of low and high nuclearity. These reactions may have a larger role in solutions reduced by BTBC, where the reducing rate coefficient is relatively slow; hence, solution reactions can contribute to cluster charge formation.

As one example, the putative, neutral, closed-shell, molecular species, $\text{Au}_8(\text{PPh}_3)\text{L}_3^3$, which is similar to the observed closed-shell, molecular cation, $[\text{Au}_8(\text{PPh}_3)\text{L}_3^3]^{2+}$, may be converted to a closed-shell cation of higher nuclearity. One such conversion scheme is



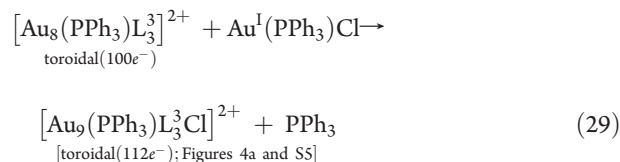
The present data allow several variations of these reactions 26, 27a, and 27b where the reactants $\text{Au}(\text{PPh}_3)\text{Cl}$, $[\text{Au}(\text{PPh}_3)\text{L}^3]^+$, $[\text{Au}(\text{PPh}_3)_2]^+$, and $[\text{Au}_2\text{L}^3\text{Cl}]^+$ appear interchangeable with respect to ion formation. As appropriate, the reaction products may yield a Cl^- leaving group instead of a phosphine ligand. This reaction scheme can process neutral species of the set, $\{\text{Au}_8(\text{PPh}_3)_x\text{L}_3^3; x + 2y = 7 \text{ or } 8\}$, into cations of higher Au nuclearity, such as the observed products: $[\text{Au}_8(\text{PPh}_3)_2\text{L}_3^3]^{2+}$, $[\text{Au}_8(\text{PPh}_3)\text{L}_3^3]^{2+}$, and $[\text{Au}_8\text{L}_4^3]^{2+}$ (Figures 2b, 4, and 6a).

When devising reaction mechanisms for use in computational simulations of nanocluster formation, one should keep in mind that the electrical charge of reactants can enhance or diminish associated reaction rates; however, charge exchange reactions may be common in solution. For example, observations of the reaction



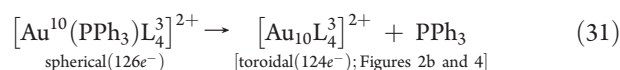
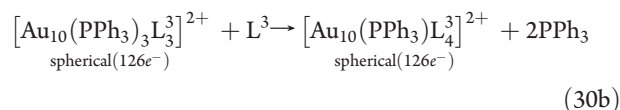
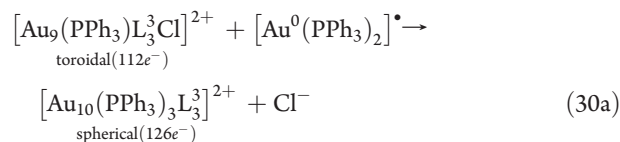
have determined the equilibrium constants of reaction 28 in CH_3CN , CH_2Cl_2 , and acetone, finding that the energy differences among the species with +1, +2, and +3 charges are small and entropy change is essentially equal to the solvent reorganization energy.^{70,100} The solution-phase relative energies of species containing L^3 may also be favorable for charge exchange. Thus, solvent-mediated processes, such as reaction 28, can facilitate formation of the lowest energy clusters.

7. Reactions That Increase Au_x Nuclearity. The concurrent disappearance of peaks corresponding to octagold clusters and the appearance of the undecagold peaks observed in the ESI-MS data for $\text{Au}:\text{L}^3$ synthesis (Figures 2 and 4) comprise putative evidence for a scheme involving core enlargement and autologous ligand exchange. Expansion of the core nuclearity can proceed through addition of monogold or digold species. For example, addition of $\text{Au}^1(\text{PPh}_3)\text{Cl}$ to $[\text{Au}_8(\text{PPh}_3)_3\text{L}_2^3]^{2+}$ can account for the early appearance of $[\text{Au}_9(\text{PPh}_3)\text{L}_3^3\text{Cl}]^{2+}$ in the ESI-MS data



Reaction 29 increases the core nuclearity; however, addition of the chloride substituent allows the cluster to maintain a minimum energy structure, according to PSEP theory.

Addition of Au^0 species can also increase nuclearity



The $[\text{Au}_{10}(\text{PPh}_3)\text{L}_4^3]^{2+}$ cluster is not observed in our data; however, our solution studies of the analogous $[\text{Au}_{10}\text{L}_4^3]^{2+}$ and

that the mechanism of chemical reactions comprising the total synthesis mechanism is a robust reaction mechanism.

Over time the dispersity of samples appears to narrow. This result is consistent with the proposed framework of converging addition and etching reactions. The reaction rates of the addition and etching process vary greatly such that the reaction mechanism favors formation of stable, closed-shell clusters. The presence of etching processes is a requirement for size-selective syntheses of monodisperse MPCs. The observation that oxygen can suppress nanocluster chlorides, thus, favoring formation of a monodisperse sample through a size-focusing process (in this case, $[\text{Au}_{11}\text{L}_3]^{3+}$), is evidence that the etching processes leading to monodisperse samples need not be confined to gold complex reagents alone.

■ ASSOCIATED CONTENT

S Supporting Information. Method for determining the optimum amount of NaBH_4 reducing reagent, reference UV–vis absorption spectra for gold clusters, measurements of colloidal agglomerates formed from primary Au_xL^3 clusters, ESI-MS data of timed Au_xL^3 cluster growth in chloroform solutions undergoing reduction by BTBC, and ESI-MS data for aerated solution at $t = 60$ days. This material is available free of charge via the Internet at <http://pubs.acs.org>.

■ AUTHOR INFORMATION

Corresponding Author

*Phone: 301-975-2512. Fax: 301-975-2643. E-mail: Jeffrey.hudgens@nist.gov

Present Addresses

^SDepartment of Chemistry and Biochemistry, Notre Dame University, Notre Dame, IN 46556-5670.

^{||}Department of Chemistry, Miami University, Oxford, OH 45056.

■ ACKNOWLEDGMENT

We thank Dr. Denis E. Bergeron for advice and help with experiments involving the aerated solutions. We thank Dr. James Falabella for advice and help with the sedimentation experiments. J.M.P. acknowledges the National Academy of Science's National Research Council for a postdoctoral fellowship. T.S. and R.B. acknowledge their support from the NIST Summer Undergraduate Research Fellowship program.

■ REFERENCES

- (1) Schmid, G. *Polyhedron* **1988**, *7*, 2321–2329.
- (2) Schmid, G. *Chem. Soc. Rev.* **2008**, *37*, 1909–1930.
- (3) Negishi, Y.; Takasugi, Y.; Sato, S.; Yao, H.; Kimura, K.; Tsukuda, T. *J. Phys. Chem. B* **2006**, *110*, 12218–12221.
- (4) Zheng, N.; Fan, J.; Stucky, G. D. *J. Am. Chem. Soc.* **2006**, *128*, 6550–6551.
- (5) Zhu, M.; Lanni, E.; Garg, N.; Bier, M. E.; Jin, R. *J. Am. Chem. Soc.* **2008**, *130*, 1138–1139.
- (6) Qian, H. F.; Zhu, M. Z.; Lanni, E.; Zhu, Y.; Bier, M. E.; Jin, R. C. *J. Phys. Chem. C* **2009**, *113*, 17599–17603.
- (7) Qian, H. F.; Jin, R. C. *Nano Lett.* **2009**, *9*, 4083–4087.
- (8) Jin, R. C.; Qian, H. F.; Wu, Z. K.; Zhu, Y.; Zhu, M. Z.; Mohanty, A.; Garg, N. *J. Phys. Chem. Lett.* **2010**, *1*, 2903–2910.
- (9) Saunders, A. E.; Sigman, M. B.; Korgel, B. A. *J. Phys. Chem. B* **2004**, *108*, 193–199.
- (10) Wang, J.; Boelens, H. F. M.; Thathagar, M. B.; Rothenberg, G. *ChemPhysChem* **2004**, *5*, 93–98.
- (11) Woehrl, G. H.; Hutchison, J. E. *Inorg. Chem.* **2005**, *44*, 6149–6158.
- (12) Negishi, Y.; Nobusada, K.; Tsukuda, T. *J. Am. Chem. Soc.* **2005**, *127*, 5261–5270.
- (13) Brennan, J. P.; Liu, X.; Dai, Q.; Worden, J. G.; Huo, Q. *J. Comput. Theor. Nanosci.* **2006**, *3*, 417–422.
- (14) Liu, X.; Worden, J. G.; Huo, Q.; Brennan, J. R. *J. Nanosci. Nanotechnol.* **2006**, *6*, 1054–1059.
- (15) Ott, L. S.; Finke, R. G. *Coord. Chem. Rev.* **2007**, *251*, 1075–1100.
- (16) Brennan, J. P.; Liu, X.; Huo, Q. *J. Comput. Theor. Nanosci.* **2007**, *4*, 127–132.
- (17) Kumar, S.; Gandhi, K. S.; Kumar, R. *Ind. Eng. Chem. Res.* **2007**, *46*, 3128–3136.
- (18) Liu, X.; Atwater, M.; Wang, J. H.; Dai, Q.; Zou, J. H.; Brennan, J. P.; Huo, Q. *J. Nanosci. Nanotechnol.* **2007**, *7*, 3126–3133.
- (19) Ott, L. S.; Finke, R. G. *Chem. Mater.* **2008**, *20*, 2592–2601.
- (20) Foos, E. E.; Twigg, M. E.; Snow, A. W.; Ancona, M. G. *J. Cluster Sci.* **2008**, *19*, 573–589.
- (21) Watzky, M. A.; Finney, E. E.; Finke, R. G. *J. Am. Chem. Soc.* **2008**, *130*, 11959–11969.
- (22) Pettibone, J. M.; Hudgens, J. W. *J. Phys. Chem. Lett.* **2010**, *1*, 2536–2540.
- (23) Bergeron, D. E.; Coskuner, O.; Hudgens, J. W.; Gonzalez, C. A. *J. Phys. Chem. C* **2008**, *112*, 12308–12814.
- (24) Pettibone, J. M.; Hudgens, J. W. *ACS Nano* **2011**, *5*, 2989–3002.
- (25) Guidez, E. B.; Hadley, A.; Aikens, C. M. *J. Phys. Chem. C* **2011**, *115*, 6305–6316.
- (26) Finney, E. E.; Finke, R. G. *J. Colloid Interface Sci.* **2008**, *317*, 351–374.
- (27) Watzky, M. A.; Finke, R. G. *J. Am. Chem. Soc.* **1997**, *119*, 10382–10400.
- (28) Hall, K. P.; Mingos, D. M. P. *Prog. Inorg. Chem.* **1984**, *32*, 237–325.
- (29) Finney, E. E.; Finke, R. G. *Chem. Mater.* **2008**, *20*, 1956–1970.
- (30) Zhang, H. F.; Stender, M.; Zhang, R.; Wang, C. M.; Li, J.; Wang, L. S. *J. Phys. Chem. B* **2004**, *108*, 12259–12263.
- (31) Negishi, Y.; Takasugi, Y.; Sato, S.; Yao, H.; Kimura, K.; Tsukuda, T. *J. Am. Chem. Soc.* **2004**, *126*, 6518–6519.
- (32) Shichibu, Y.; Negishi, Y.; Tsukuda, T.; Teranishi, T. *J. Am. Chem. Soc.* **2005**, *127*, 13464–13465.
- (33) Bertino, M. F.; Sun, Z. M.; Zhang, R.; Wang, L. S. *J. Phys. Chem. B* **2006**, *110*, 21416–21418.
- (34) Yanagimoto, Y.; Negishi, Y.; Fujihara, H.; Tsukuda, T. *J. Phys. Chem. B* **2006**, *110*, 11611–11614.
- (35) Duan, H. W.; Nie, S. M. *J. Am. Chem. Soc.* **2007**, *129*, 2412–2413.
- (36) Negishi, Y.; Chaki, N. K.; Shichibu, Y.; Whetten, R. L.; Tsukuda, T. *J. Am. Chem. Soc.* **2007**, *129*, 11322–11323.
- (37) Bergeron, D. E.; Hudgens, J. W. *J. Phys. Chem. C* **2007**, *111*, 8195–8201.
- (38) Tracy, J. B. C.; M., C.; Parker, J. F.; Hampe, O.; Fields-Zinna, C. A.; Dass, A.; Murray, R. W. *J. Am. Chem. Soc.* **2007**, *129*, 16209–16215.
- (39) Golightly, J. S.; Gao, L.; Castleman, A. W.; Bergeron, D. E.; Hudgens, J. W.; Magyar, R. J.; Gonzalez, C. A. *J. Phys. Chem. C* **2007**, *111*, 14625–14627.
- (40) Tracy, J. B.; Kalyuzhny, G.; Crowe, M. C.; Balasubramanian, R.; Choi, J. P.; Murray, R. W. *J. Am. Chem. Soc.* **2007**, *129*, 6706–6707.
- (41) Tracy, J. B.; Crowe, M. C.; Parker, J. F.; Hampe, O.; Fields-Zinna, C. A.; Dass, A.; Murray, R. W. *J. Am. Chem. Soc.* **2007**, *129*, 16209–16215.
- (42) Gies, A. P.; Hercules, D. M.; Gerdon, A. E.; Cliffl, D. E. *J. Am. Chem. Soc.* **2007**, *129*, 1095–1104.
- (43) Chaki, N. K.; Negishi, Y.; Tsunoyama, H.; Shichibu, Y.; Tsukuda, T. *J. Am. Chem. Soc.* **2008**, *130*, 8608–8610.
- (44) Rodriguez, L.; Lodeiro, C.; Lima, J. C.; Crehuet, R. *Inorg. Chem.* **2008**, *47*, 4952–4962.

- (45) Fields-Zinna, C. A.; Sampson, J. S.; Crowe, M. C.; Tracy, J. B.; Parker, J. F.; deNey, A. M.; Muddiman, D. C.; Murray, R. W. *J. Am. Chem. Soc.* **2009**, *131*, 13844–13851.
- (46) Kimura, K.; Sugimoto, N.; Sato, S.; Yao, H.; Negishi, Y.; Tsukuda, T. *J. Phys. Chem. C* **2009**, *113*, 14076–14082.
- (47) Fields-Zinna, C. A.; Crowe, M. C.; Dass, A.; Weaver, J. E. F.; Murray, R. W. *Langmuir* **2009**, *25*, 7704–7710.
- (48) Zhou, R. J.; Shi, M. M.; Chen, X. Q.; Wang, M.; Chen, H. Z. *Chem.—Eur. J.* **2009**, *15*, 4944–4951.
- (49) Certain commercial materials and equipment are identified in this paper in order to adequately specify the experimental procedure. Such identification implies neither recommendation or endorsement by the National Institute of Standards and Technology nor that the material or equipment identified is the best available for the purpose.
- (50) The equilibration time of 15 min was determined from a set of ESI-MS measurements. Au(PPh₃)Cl and L³ were added to solvent and stirred, and small samples were withdrawn for ESI-MS analyses. For the reagent weights and solvent volumes used, the ratio of ion abundances ceased to vary before 15 min passed. Thus, samples were allowed at least 15 min to equilibrate.
- (51) Zhou, S. L.; Hamburger, M. *Rapid Commun. Mass Spectrom.* **1996**, *10*, 797–800.
- (52) Davis, R. E.; Gottbrath, J. A. *J. Am. Chem. Soc.* **1962**, *84*, 895–898.
- (53) Brown, H. C.; Mead, E. J.; Rao, B. C. S. *J. Am. Chem. Soc.* **1955**, *77*, 6209–6213.
- (54) Standard deviations for the data in the figures were examined. In most cases, we found $\sigma < 1\%$. Maximal standard deviations were found at intermediate concentration ratios; in all cases, we found $\sigma < 10\%$. These deviations did not in any way obscure the overall trends.
- (55) Di Marco, V. B.; Bombi, G. G. *Mass Spectrom. Rev.* **2006**, *25*, 347–379.
- (56) Wang, J. C. *Acta Crystallogr., Sect. C: Cryst. Struct. Commun.* **1996**, *52*, 611–613.
- (57) Porter, L. C.; Khan, N. I.; King, C.; Fackler, J. P. *Acta Crystallogr., Sect. C: Cryst. Struct. Commun.* **1989**, *45*, 947–949.
- (58) Yam, V. W. W.; Lai, T. F.; Che, C. M. *J. Chem. Soc., Dalton Trans.* **1990**, 3747–3752.
- (59) Li, D.; Che, C. M.; Peng, S. M.; Liu, S. T.; Zhou, Z. Y.; Mak, T. C. W. *J. Chem. Soc., Dalton Trans.* **1993**, 189–194.
- (60) Zeller, E.; Beruda, H.; Schmidbaur, H. *Inorg. Chem.* **1993**, *32*, 3203–3204.
- (61) van der Velden, J. W. A.; Vollenbroek, F. A.; Bour, J. J.; Beurskens, P. T.; Smits, J. M. M.; Bosman, W. P. *Recl. Trav. Chim. Pays-Bas* **1981**, *100*, 148–152.
- (62) van der Velden, J. W. A.; Bour, J. J.; Steggerda, J. J.; Beurskens, P. T.; Roseboom, M.; Noordik, J. H. *Inorg. Chem.* **1982**, *21*, 4321–4324.
- (63) Briant, C. E.; Hall, K. P.; Mingos, D. M. P. *J. Organomet. Chem.* **1983**, *254*, C18–C20.
- (64) van der Velden, J. W. A.; Beurskens, P. T.; Bour, J. J.; Bosman, W. P.; Noordik, J. H.; Kolenbrander, M.; Buskes, J. *Inorg. Chem.* **1984**, *23*, 146–151.
- (65) van der Velden, J. W. A.; Bour, J. J.; Bosman, W. P.; Noordik, J. H. *J. Chem. Soc. D: Chem. Commun.* **1981**, 1218–1219.
- (66) Manassero, M.; Naldini, L.; Sansoni, M. *J. Chem. Soc. D: Chem. Commun.* **1979**, 385–386.
- (67) Bellon, P. L.; Cariati, F.; Manasser, M.; Naldini, L.; Sansoni, M. *J. Chem. Soc. D: Chem. Commun.* **1971**, 1423–1424.
- (68) Schulz-Dobrick, M.; Jansen, M. *Eur. J. Inorg. Chem.* **2006**, 4498–4502.
- (69) Wen, F.; Englert, U.; Gutrath, B.; Simon, U. *Eur. J. Inorg. Chem.* **2008**, 106–111.
- (70) van der Velden, J. W. A.; Bour, J. J.; Bosman, W. P.; Noordik, J. H.; Beurskens, P. T. *Recl. Trav. Chim. Pays-Bas* **1984**, *103*, 13–16.
- (71) Briant, C. E.; Hall, K. P.; Wheeler, A. C.; Mingos, D. M. P. *J. Chem. Soc. D: Chem. Commun.* **1984**, 248–250.
- (72) Smits, J. M. M.; Bour, J. J.; Vollenbroek, F. A.; Beurskens, P. T. *J. Crystallogr. Spectrosc. Res.* **1983**, *13*, 355–363.
- (73) Briant, C. E.; Theobald, B. R. C.; White, J. W.; Bell, L. K.; Mingos, D. M. P.; Welch, A. J. *J. Chem. Soc. D: Chem. Commun.* **1981**, 201–202.
- (74) Kebarle, P. *J. Mass Spectrom.* **2000**, *35*, 804–817.
- (75) Kebarle, P.; Peschke, M. *Anal. Chim. Acta* **2000**, *406*, 11–35.
- (76) Kebarle, P.; Verkerk, U. H. *Mass Spectrom. Rev.* **2009**, *28*, 898–917.
- (77) Kebarle, P.; Verkerk, U. H. On the Mechanism of Electrospray Ionization Mass Spectrometry (ESI-MS). In *Electrospray and MALDI Mass Spectrometry: Fundamentals, Instrumentation, Practicalities, and Biological Applications*; 2nd ed.; Cole, R. B., Ed.; John Wiley & Sons, Inc.: Hoboken, 2010; pp 3–48.
- (78) Cole, R. B. *J. Mass Spectrom.* **2000**, *35*, 763–772.
- (79) Cech, N. B.; Enke, C. G. *Mass Spectrom. Rev.* **2001**, *20*, 362–387.
- (80) Enke, C. G. *Anal. Chem.* **1997**, *69*, 4885–4893.
- (81) van der Velden, J. W. A.; Bour, J. J.; Bosman, W. P.; Noordik, J. H. *Inorg. Chem.* **1983**, *22*, 1913–1918.
- (82) In ref 62 van der Velden et al. prepared [Au₆L₄](NO₃)₂ by reaction of Au₄(PPh₃)₄I₂ in a solution containing excess L³; however, we ignore this source reaction, as it is not available in this system.
- (83) IUPAC. *Compendium of Chemical Terminology (the “Gold Book”)*, 2nd ed.; McNaught, A. D., Wilkinson, A., Eds.; Blackwell Scientific Publications: Oxford, 1997. XML on-line-corrected version: <http://goldbook.iupac.org> (2006) created by Nic, M.; Jirat, J.; Kosata, B. updates compiled by Jenkins, A. ISBN 0-9678550-9-8. doi:10.1351/goldbook, 2006.
- (84) Pan, Q. J.; Zhou, X.; Guo, Y. R.; Fu, H. G.; Zhang, H. X. *Inorg. Chem.* **2009**, *48*, 2844–2854.
- (85) King, R. B. *Inorg. Chim. Acta* **1986**, *116*, 109–117.
- (86) Schwerdtfeger, P.; Hermann, H. L.; Schmidbaur, H. *Inorg. Chem.* **2003**, *42*, 1334–1342.
- (87) Evans, D. G.; Mingos, D. M. P. *J. Organomet. Chem.* **1982**, *232*, 171–191.
- (88) Mingos, D. M. P. *Philos. Trans. R. Soc. A* **1982**, *308*, 75–83.
- (89) Lo, C. T. F.; Karan, K.; Davis, B. R. *Ind. Eng. Chem. Res.* **2007**, *46*, 5478–5484.
- (90) Brown, H. C.; Mead, E. J.; Shoaf, C. J. *J. Am. Chem. Soc.* **1956**, *78*, 3616–3620.
- (91) Majimel, J.; Bacinello, D.; Durand, E.; Vallee, F.; Treguer-Delapierre, M. *Langmuir* **2008**, *24*, 4289–4294.
- (92) Elian, M.; Chen, M. M. L.; Mingos, D. M. P.; Hoffmann, R. *Inorg. Chem.* **1976**, *15*, 1148–1155.
- (93) Mingos, D. M. P.; Slee, T.; Lin, Z. Y. *Chem. Rev.* **1990**, *90*, 383–402.
- (94) Mingos, D. M. P. *J. Chem. Soc., Dalton Trans.* **1976**, 1163–1169.
- (95) Mingos, D. M. P. *Polyhedron* **1984**, *3*, 1289–1297.
- (96) Mingos, D. M. P. *J. Chem. Soc., Dalton Trans.* **1996**, 561–566.
- (97) Pyykkö, P. *Angew. Chem., Int. Ed.* **2004**, *43*, 4412–4456.
- (98) Shafai, G.; Hong, S.; Bertino, M. F.; Rahman, T. S. *J. Phys. Chem. C* **2009**, *113*, 12072–12078.
- (99) Vollenbroek, F. A.; Bour, J. J.; Vandervelden, J. W. A. *Recl. Trav. Chim. Pays-Bas* **1980**, *99*, 137–141.
- (100) Van der Linden, J. G. M.; Paulissen, M. L. H.; Schmitz, J. E. J. *J. Am. Chem. Soc.* **1983**, *105*, 1903–1907.
- (101) Cheetham, G. M. T.; Harding, M. M.; Haggitt, J. L.; Mingos, D. M. P.; Powell, H. R. *J. Chem. Soc. D: Chem. Commun.* **1993**, 1000–1001.
- (102) Laguna, A.; Laguna, M.; Gimeno, M. C.; Jones, P. G. *Organometallics* **1992**, *11*, 2759–2760.
- (103) Hoffmann, R. *Angew. Chem., Int. Ed. Engl.* **1982**, *21*, 711–724.
- (104) Wang, B. S.; Hou, H.; Yoder, L. M.; Muckerman, J. T.; Fockenberg, C. *J. Phys. Chem. A* **2003**, *107*, 11414–11426.
- (105) Hong, S.; Shafai, G.; Bertino, M.; Rahman, T. S. *J. Phys. Chem. C* **2011**, *115*, 14478–14487.